Chapter 7
Layered and Truncated Conductors

Abstract The subject of this chapter is the eddy-current inspection of test-pieces that are coated, layered, or truncated. It is presumed that various surfaces of the test-piece significantly perturb the induced eddy currents and that the effect of those surfaces must be taken into account to properly interpret the observed eddy-current probe coil impedance. The discussion includes a description of impedance-plane diagrams for surface coils, encircling coils, and bobbin coils in relation to coated, layered, or truncated test-pieces with planar or cylindrical surfaces. The effect of the test-piece edge on the observed probe coil impedance is also described.

7.1 Introduction

In this chapter, the effect on the impedance of the eddy-current coil of a test-piece with multiple physical boundaries or interfaces is discussed. In Chap. 6, the discussion was limited to fundamental cases described by one physical boundary—either flat or cylindrical—at the surface of a homogeneous conductor. Generally, coil impedance can be expressed for an arbitrary number of layers in the sample, each with its particular material properties σ_i and μ_i. Such expressions of impedance are presented here for a multilayered test-piece, whose interfaces are all (i) parallel planes and (ii) concentric cylinders. Impedance expressions are also presented for cases that are important in practical terms, i.e., for simplified geometries in which the test-piece has two layers. One of these cases is that of the coated conductor; a half-space or cylinder with a coating which may or may not be conductive, and the other case is that of the plate or tube; a conductor of finite thickness. It is worth acknowledging that no conductor is truly a half-space, i.e., infinitely thick, but in the context of EC NDE a half-space is a conductor with a planar inspection surface, whose other surfaces (sides and back-plane) are sufficiently remote that they do not disturb the eddy currents significantly. As in Chap. 6, the spherical test-piece geometry is not discussed explicitly here. Readers interested in a treatment of eddy-current probe response to layered spheres are directed to [1, 2].

In Sect. 7.2, expressions are provided for the impedance of coils that exhibit cylindrical symmetry in relation to these test-pieces. In Sect. 7.3, a description is

N. Bowler, *Eddy-Current Nondestructive Evaluation*,
Springer Series in Measurement Science and Technology,
https://doi.org/10.1007/978-1-4939-9629-2_7

provided of methods that can be applied to analyze inspection scenarios in which the conductors are truncated in some manner; a plate edge or the end of a tube, for example. Impedance-plane plots are presented in several cases.

For geometries yet more complex than these, such as a coil interacting with a rivet in a layered aircraft skin, full numerical modeling in the form of finite- or boundary-element approaches are applicable. Numerous approaches to computational electromagnetics in the context of EC NDE are discussed by Sabbagh et al. [3].

7.2 Layered Conductors

The important work of Dodd and Deeds published in 1968 [4] involves analyses of the impedance of a surface coil positioned above a half-space conductor, discussed in Sect. 6.3.4, and of a coil encircling a rod conductor, discussed in Sect. 6.5.2. In both configurations, the treatment presented in [4] accommodates a single surface layer of a different material coating the test-piece. In fact, since the material properties assigned to the surface layer or substrate are entirely arbitrary in the analysis, the impedance of a surface coil positioned above a plate or of a coil encircling a tube conductor can also be computed by assigning the conductivity of the substrate to be zero. Extending this work to test-pieces with an arbitrary number of layers, co-author Cheng joined Dodd and Deeds and published analyses in 1971 and 1974 concerning the impedance of an eddy current surface coil above a planar conductor composed of an arbitrary number of layers [5] and of an eddy current coil coaxial with an arbitrary number of cylindrical conductors [6]. The former, [5], is useful not only for studying the impedance of a surface coil in the vicinity of a layered planar conductor, discussed in Sect. 7.2.1, but also of a plate sufficiently thin for its back surface to influence the value of measured coil impedance, which itself might be composed of multiple layers. The latter, [6], is applicable to a coil encircling a solid circular cylindrical conductor, discussed in Sect. 6.5.2, and to a coil internal to and coaxial with a borehole in a conductor. The fact that an arbitrary number of cylindrical conductors is treated, Sect. 7.2.4, allows the analysis to be applied also to a coil external to a layered cylindrical rod, Sect. 7.2.5, to a coil coaxial with a tube (either internal or external), Sect. 7.2.6, and to a coil internal to a layered borehole, not discussed explicitly in this text.

7.2.1 Planar Conductor with an Arbitrary Number of Layers

The impedance of a surface coil positioned above a planar conductor with an arbitrary number of layers, shown schematically in Fig. 7.1, is given by

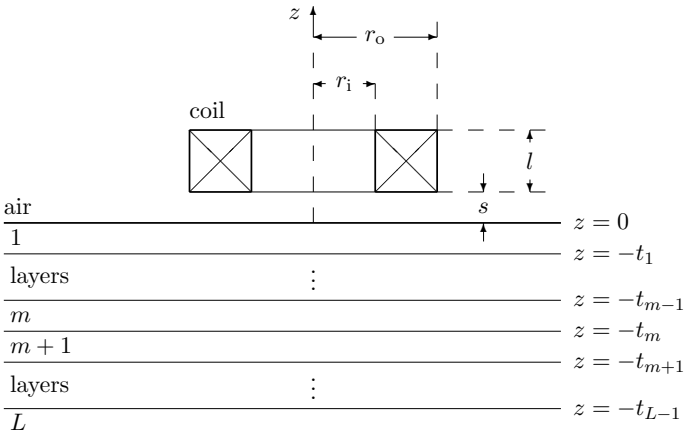

Fig. 7.1 Cross-section through the axis of a circular, air-cored, eddy-current surface coil, positioned above a layered half-space

$$Z = \frac{j\omega\mu_0\pi n^2}{l^2(r_o - r_i)^2}\int_0^\infty \frac{J^2(\kappa r_i, \kappa r_o)}{\kappa^6}\left\{2\kappa l + 2e^{-\kappa l} - 2 + \left[e^{-\kappa s} - e^{-\kappa(s+l)}\right]^2 \times\left[\frac{(\kappa\mu_{r(m+1)} - \gamma_1)V_{11}(1) + (\kappa\mu_{r(m+1)} + \gamma_1)V_{21}(1)}{(\kappa\mu_{r(m+1)} + \gamma_1)V_{11}(1) + (\kappa\mu_{r(m+1)} - \gamma_1)V_{21}(1)}\right]\right\} d\kappa \quad (7.1)$$

where $\gamma_i = \sqrt{\kappa^2 + j\omega\mu_0\mu_{ri}\sigma_i}$ and μ_{ri} is the relative permeability of the ith layer. The first three terms in curly brackets $2\kappa l + 2e^{-\kappa l} - 2$, in (7.1) give the impedance of the isolated coil (6.88). The remainder of the expression represents the additional effect of the conductor on the coil impedance. In (7.1), the function $J(\kappa r_i, \kappa r_o)$ defined in (6.78) is related to the coil dimensions. The matrix elements $V_{kl}(k, l = 1, 2)$ have argument m, where m is an integer denoting the position of the layer relative to the coil. Then,

$$\overline{V}(m) = \overline{T}(m, m+1)\overline{T}(m+1, m+2)\ldots\overline{T}(L-2, L-1)\overline{T}(L-1, L) \quad (7.2)$$

where the $\overline{T}(m, m+1)$ are 2×2 transformation matrices

$$\overline{T}(m, m+1) = \begin{bmatrix} T_{11}(m, m+1) & T_{12}(m, m+1) \\ T_{21}(m, m+1) & T_{22}(m, m+1) \end{bmatrix} \quad (7.3)$$

whose elements are

$$T_{11}(m, m+1) = \frac{1}{2}e^{(-\gamma_{m+1}+\gamma_m)t_m}\left[1 + \frac{\mu_{rm}}{\mu_{r(m+1)}}\frac{\gamma_{m+1}}{\gamma_m}\right]$$

$$T_{12}(m, m+1) = \frac{1}{2}e^{(\gamma_{m+1}+\gamma_m)t_m}\left[1 - \frac{\mu_{rm}}{\mu_{r(m+1)}}\frac{\gamma_{m+1}}{\gamma_m}\right]$$

$$T_{21}(m, m+1) = \frac{1}{2} e^{(-\gamma_{m+1}-\gamma_m)t_m} \left[1 - \frac{\mu_{rm}}{\mu_{r(m+1)}} \frac{\gamma_{m+1}}{\gamma_m}\right]$$
$$T_{22}(m, m+1) = \frac{1}{2} e^{(\gamma_{m+1}-\gamma_m)t_m} \left[1 + \frac{\mu_{rm}}{\mu_{r(m+1)}} \frac{\gamma_{m+1}}{\gamma_m}\right]. \quad (7.4)$$

7.2.2 Coated Half-Space Conductor

The case of the half-space conductor with a surface coating of another material, or with a surface that has been modified by a particular treatment process (e.g., surface hardening), is commonly encountered in practice. Such a test-piece can often be considered as having a step-function change in material properties at the interface between the two media. The impedance change of an air-cored surface coil positioned above a coated half-space can be deduced from (7.1) by putting $L = 2$:

$$Z = \frac{2j\omega\mu_0\pi n^2}{l^2(r_o - r_i)^2} \int_0^\infty \frac{J^2(\kappa r_i, \kappa r_o)}{\kappa^6} \left\{\kappa l + e^{-\kappa l} - 1 + \left[e^{-\kappa s} - e^{-\kappa(s+l)}\right]^2 \times \left[\frac{(\gamma_1\mu_{r2} + \gamma_2\mu_{r1})(\kappa\mu_{r1} - \gamma_1) + e^{-2\gamma_1 t_1}(\gamma_1\mu_{r2} - \gamma_2\mu_{r1})(\kappa\mu_{r1} + \gamma_1)}{(\gamma_1\mu_{r2} + \gamma_2\mu_{r1})(\kappa\mu_{r1} + \gamma_1) + e^{-2\gamma_1 t_1}(\gamma_1\mu_{r2} - \gamma_2\mu_{r1})(\kappa\mu_{r1} - \gamma_1)}\right]\right\} d\kappa \quad (7.5)$$

The normalized impedance plane diagram Fig. 7.2 illustrates how the impedance of an air-cored coil changes as a function of the thickness of a conductive coating on a half-space substrate of different conductivity.

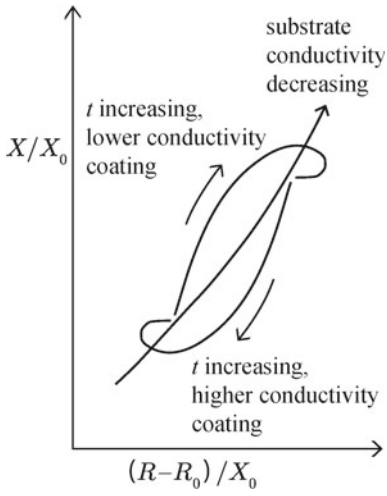

Fig. 7.2 Normalized impedance plane diagram for an air-cored surface coil positioned above a coated half-space. The normalized impedance depends upon the coating thickness, its conductivity, and the conductivity of the half-space substrate. Both the substrate and coating are non-ferromagnetic in this example

7.2.3 Plate Conductor

The impedance of an air-cored surface coil positioned above a layered plate can be deduced from (7.1) by putting $\sigma_L = 0$ and $\mu_{rL} = 1$. With these parameters, the second-line term in (7.1) in square brackets becomes simply $[V_{21}(1)/V_{11}(1)]$.

The impedance of a coil in the presence of a homogeneous plate is a special case that combines the conditions $L = 2$, $\sigma_L = \sigma_2 = 0$ and $\mu_{rL} = \mu_{r2} = 1$. Imposing these values in (7.1) or (7.5) gives

$$Z = \frac{2j\omega\mu_0\pi n^2}{l^2(r_\mathrm{o}-r_\mathrm{i})^2}\int_0^\infty \frac{J^2(\kappa r_\mathrm{o},\kappa r_\mathrm{i})}{\kappa^6}\left\{\kappa l + e^{-\kappa l} - 1 + \left[e^{-\kappa s} - e^{-\kappa(s+l)}\right]^2 \times \left[\frac{(\gamma_1+\kappa\mu_{r1})(\kappa\mu_{r1}-\gamma_1) + e^{-2\gamma_1 t_1}(\gamma_1-\kappa\mu_{r1})(\kappa\mu_{r1}+\gamma_1)}{(\gamma_1+\kappa\mu_{r1})(\kappa\mu_{r1}+\gamma_1) + e^{-2\gamma_1 t_1}(\gamma_1-\kappa\mu_{r1})(\kappa\mu_{r1}-\gamma_1)}\right]\right\} d\kappa. \quad (7.6)$$

An impedance plane plot showing the effect of changing the thickness of various metal plates on the impedance of a surface coil is given in Fig. 7.3. It is noticeable that the resistance of the coil passes through a maximum value as the thickness of the test-piece increases, whereas the coil reactance passes through a minimum, before the coil impedance converges to a constant complex value equal to its impedance in the presence of a half-space conductor. Convergence occurs as the conductor becomes sufficiently thick that its back wall no longer disturbs the eddy-current distribution significantly. The way in which increasing conductivity or lift-off affects the impedance is marked in Fig. 7.3 and has already been discussed in the context of Fig. 6.2.

7.2.4 Cylindrical Conductor with an Arbitrary Number of Layers

The impedance of a coil coaxial with an arbitrary number of conductive layers that may be located exterior and/or interior to it, shown schematically in Fig. 7.4, is given by

$$Z = Z_0 + \frac{2j\omega\mu_0 n^2}{l^2(r_\mathrm{o}-r_\mathrm{i})^2}\int_0^\infty \frac{2(1-\cos\kappa l)}{\kappa^6} \times \left[\frac{U_{12}V_{11}I^2(\kappa r_\mathrm{i},\kappa r_\mathrm{o}) + U_{22}V_{21}K^2(\kappa r_\mathrm{i},\kappa r_\mathrm{o}) + 2U_{12}V_{21}I(\kappa r_\mathrm{i},\kappa r_\mathrm{o})K(\kappa r_\mathrm{i},\kappa r_\mathrm{o})}{U_{22}V_{11} - U_{12}V_{21}}\right] d\kappa \quad (7.7)$$

where Z_0 represents the impedance of the isolated coil, (6.88), and the second term represents the effect of the conductor on the coil impedance. The function $K^2(x_1, x_2)$ is defined in (6.130) and $I^2(x_1, x_2)$ can be obtained from it by substituting I for K.

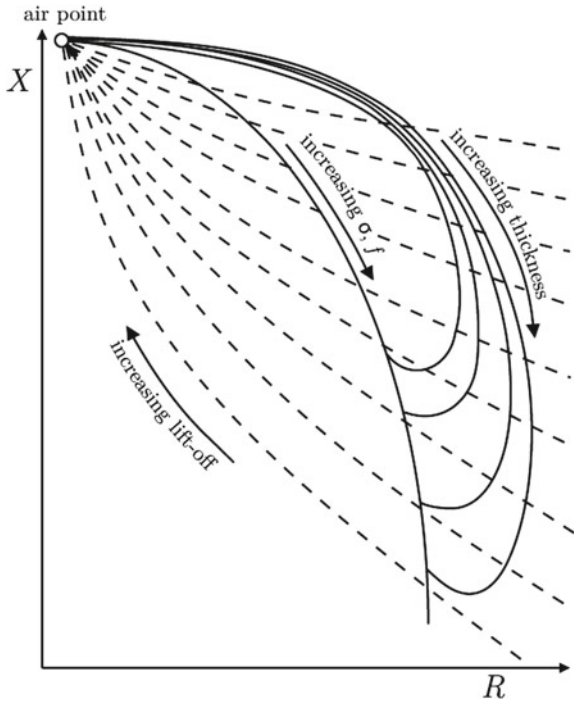

Fig. 7.3 Z for several different non-ferromagnetic metals as a function of plate thickness [7]

The matrix elements V_{ij} and U_{ij} have arguments m and m', respectively, where m and m' are integers denoting the layers adjacent to the coil, on the interior and exterior, respectively. Then,

$$\overline{V}(m) = \overline{T}(m, m-1)\overline{T}(m-1, m-2)\ldots\overline{T}(3,2)\overline{T}(2,1) \tag{7.8}$$

$$\overline{U}(m') = \overline{T}(m', m'-1)\overline{T}(m'-1, m'-2)\ldots\overline{T}(3',2')\overline{T}(2',1'), \tag{7.9}$$

where the $\overline{T}(i, j)$ are 2×2 transformation matrices

$$\overline{T}(m+1, m) = \begin{bmatrix} T_{11}(m+1, m) & T_{12}(m+1, m) \\ T_{21}(m+1, m) & T_{22}(m+1, m) \end{bmatrix}, \tag{7.10}$$

whose elements are

$$\begin{aligned} T_{11}(m+1, m) = \gamma_{m+1}\rho_m[&K_0(\gamma_{m+1}\rho_m)I_1(\gamma_m\rho_m) \\ &+(\gamma_m/\gamma_{m+1})I_0(\gamma_m\rho_m)K_1(\gamma_{m+1}\rho_m)] \\ T_{12}(m+1, m) = \gamma_{m+1}\rho_m[&K_0(\gamma_{m+1}\rho_m)K_1(\gamma_m\rho_m) \\ &+(\gamma_m/\gamma_{m+1})K_0(\gamma_m\rho_m)K_1(\gamma_{m+1}\rho_m)] \end{aligned}$$

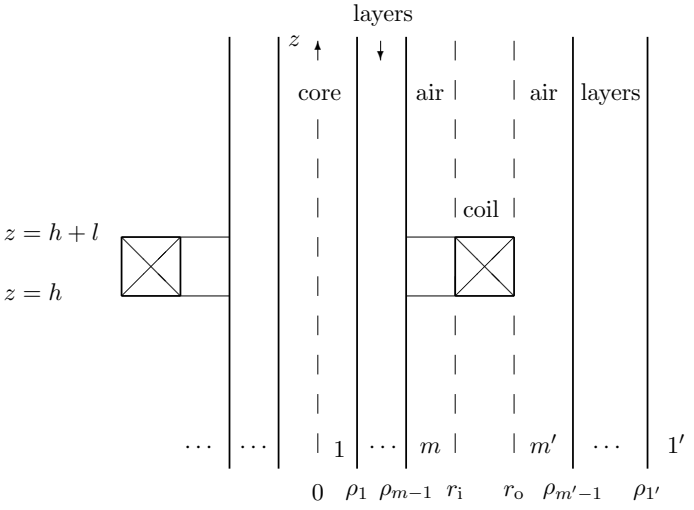

Fig. 7.4 Cross-section through the axis of a circular coil with finite cross-section, coaxial with a cylindrical conductor with an arbitrary number of layers, that may be interior (m layers) and/or exterior (m' layers) to the coil. Note that the system is circularly symmetric about the z-axis although the m' exterior layers are shown only on the right in this diagram, for clarity. $\cdots$ indicate multiple layers. Further, $r_\mathrm{i} \equiv \rho_m$ and $r_\mathrm{o} \equiv \rho_{m'}$

$$
\begin{aligned}
T_{21}(m+1,m) &= \gamma_{m+1}\rho_m[I_0(\gamma_{m+1}\rho_m)I_1(\gamma_m\rho_m) \\
&\qquad +(\gamma_m/\gamma_{m+1})I_0(\gamma_m\rho_m)I_1(\gamma_{m+1}\rho_m)] \\
T_{22}(m+1,m) &= \gamma_{m+1}\rho_m[I_0(\gamma_{m+1}\rho_m)K_1(\gamma_m\rho_m) \\
&\qquad +(\gamma_m/\gamma_{m+1})K_0(\gamma_m\rho_m)I_1(\gamma_{m+1}\rho_m)]. \quad (7.11)
\end{aligned}
$$

Note that $\overline{V}(2) = \overline{T}(2,1)$ so that $V_{11}(2)$ is simply $T_{11}(2,1)$ and $V_{21}(2)$ is $T_{21}(2,1)$, etc.

7.2.5 Coated Cylindrical Conductor

The case of the coated cylindrical conductor is useful for analyzing several configurations of practical importance such as case-hardened steel shafts, for which the surface-hardened layer has a different conductivity and permeability than the unhardened core, and metal coatings applied to rods of other metal types, for various purposes. Note that a *non*conductive (and non-ferromagnetic) coating on a cylindrical metal test-piece behaves, from the point of view of eddy-current inspection, merely as nonresponsive filler between the coil and the metal. Assuming that the

outer diameter of the test-piece can be measured, the thickness of the nonconductive coating can be determined by measuring the impedance of an encircling coil and establishing the fill-factor (and therefore radius) of the conductive core within the coil, from an impedance-plane plot such as that shown in Fig. 6.23.

For a coil encircling a coated cylinder such as that shown schematically in Fig. 7.5, the impedance is given by setting $m = 3$ and $m' = 1$ in (7.7). Noting that the following hold, in the special case of no conductive layers exterior to the coil,

$$\overline{U} = 1, \qquad \text{i.e.} \qquad U_{12} = 0 \quad \text{and} \quad U_{22} = 1, \tag{7.12}$$

then

$$Z = Z_0 + \frac{2j\omega\mu_0 n^2}{l^2(r_\mathrm{o} - r_\mathrm{i})^2} \int_0^\infty \frac{2(1 - \cos\kappa l)}{\kappa^6} \frac{V_{21}(3)}{V_{11}(3)} K^2(\kappa r_\mathrm{i}, \kappa r_\mathrm{o}) d\kappa \tag{7.13}$$

in which, explicitly,

$$V_{11}(3) = T_{11}(3,2)T_{11}(2,1) + T_{12}(3,2)T_{21}(2,1)$$
$$V_{12}(3) = T_{21}(3,2)T_{11}(2,1) + T_{22}(3,2)T_{21}(2,1)$$

and expressions for the $T_{ij}(m+1, m)$ are given in (7.11). Note, some simplification occurs for the case shown in Fig. 7.5 due to the fact that $\gamma_3 = \kappa$.

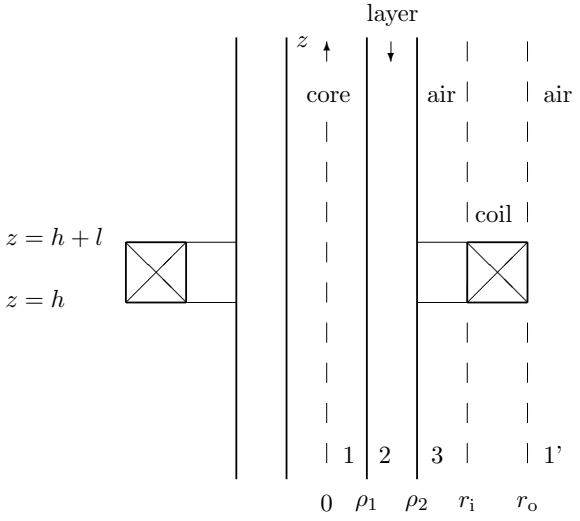

Fig. 7.5 Cross-section through the axis of a circular coil with finite cross-section, coaxial with a coated cylindrical conductor

7.2.6 Tube Conductor

Encircling Coil

For an introductory discussion on the role of the encircling coil, the reader is referred to Sect. 6.5. There, the impedance of a coil encircling a solid cylindrical rod is discussed. Here, the discussion is extended to the coil encircling a hollow cylindrical rod (cylindrical tube). As with the rod, the tube test-piece geometry was studied extensively by Friedrich Förster and a summary of his work relevant to the encircling coil and tube is given in [8, Sect. 4: Theory of Encircling Coil and Internal Axial Coil Tests of Tubes]. The definition of fill-factor given in (6.97) for the solid rod conveys the same meaning in the case of the tube but is modified according to the nomenclature of Fig. 7.5, by replacing ρ_1 in (6.97) with ρ_2, which is the outer radius of the tube indicated in Fig. 7.5:

$$\eta = \left(\frac{\rho_2}{r_\mathrm{i}}\right)^2. \tag{7.14}$$

The tube inspected by an encircling coil is a special case of the coated cylindrical conductor shown in Fig. 7.5, in which the core, region 1, takes the parameter values of air; $\sigma_1 = 0$ and $\mu_{\mathrm{r}1} = 1$ so that $\gamma_1 = \gamma_3 = \kappa$ in the equations of Sect. 7.2.5.

The normalized impedance plane diagram shown in Fig. 7.6 illustrates the effect of changing fill-factor, frequency of inspection, and test-piece conductivity for the encircling coil inspection of a conductive, non-ferromagnetic tube assuming that the coil and tube are coaxial with one another [8]. Figure 7.7 illustrates the effect on the impedance-plane plot of changing the tube wall thickness.

Bobbin Coil

For discussions on the role of the bobbin probe, the reader is referred to Sects. 6.6 and 8.3 of this text and again to the detailed work of Friedrich Förster [8, Sect. 4: Theory of Encircling Coil and Internal Axial Coil Tests of Tubes]. The definition of fill-factor given in (6.132) is modified for this case by replacing ρ_1 in (6.132) with $\rho_{m'-1}$ that denotes the inner radius of the tube shown in Fig. 7.4:

$$\eta_b = \left(\frac{r_\mathrm{o}}{\rho_{m'-1}}\right)^2. \tag{7.15}$$

The tube inspected by a bobbin coil is a special case of the coated cylindrical conductor shown in Fig. 7.4, in which there is no conductor interior to the coil and, exterior to the coil, $m' = 3$, $\sigma_{1'} = \sigma_{3'} = 0$ and $\mu_{\mathrm{r}1'} = \mu_{\mathrm{r}3'} = 1$ so that $\gamma_{1'} = \gamma_{3'} = \kappa$ in the equations of Sect. 7.2.5.

The normalized impedance-plane diagram shown in Fig. 7.6 illustrates the effect of changing fill-factor, frequency of inspection, and test-piece conductivity for the bobbin coil inspection of a conductive, non-ferromagnetic tube assuming that the

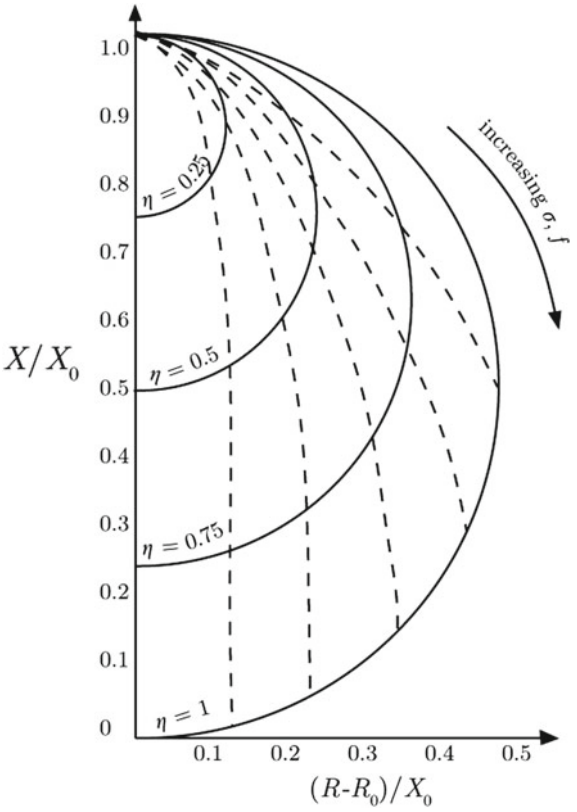

Fig. 7.6 Normalized impedance-plane plot for a coil with inner radius r_i encircling a tubular, non-ferromagnetic, test-piece with outer radius ρ_2 and constant ratio of wall thickness to ρ_2, i.e., $(\rho_2 - \rho_1)/\rho_2 = \text{constant}$, Fig. 7.5. Solid lines (——) represent the complex impedance of the probe as a function of rod conductivity, σ, or frequency of coil operation, f. Broken lines (- - -) represent the effect of changing η, (7.14). The same curves are obtained for a bobbin coil with outer radius r_o internal to and coaxial with a tube with inner diameter $\rho_{m'-1}$, Fig. 7.4 and (7.15) [8]

coil and tube are coaxial with one another [8]. Figure 7.7 illustrates the effect on the impedance-plane plot of changing the tube wall thickness.

7.3 Truncated Conductors

An eddy current probe may be viewed as 'small' relative to the dimensions of a test-piece if the eddy current density induced by the coil is negligible in the vicinity of any sharp geometrical changes in the test-piece. This condition may be satisfied if the geometrical variations of the test-piece take place over a length scale much larger than the dimensions of the probe coil, but the distribution of the eddy-current density also depends on the frequency at which the coil is operating. Looking back at Fig. 2.8 it can be seen that not only does the depth of penetration of the eddy currents decline as the frequency increases, by the skin effect, but the lateral spread of the eddy-current density declines as the probe frequency increases, as well. This

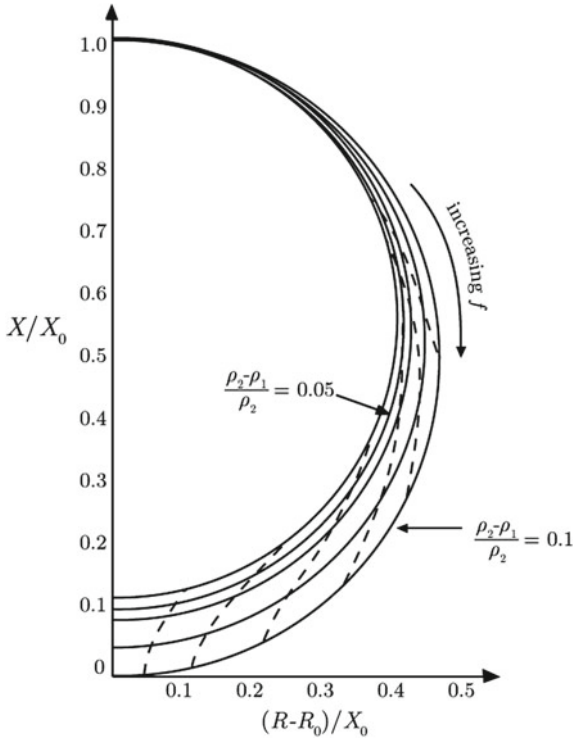

Fig. 7.7 Normalized impedance-plane plot for a coil with inner radius r_i encircling a cylindrical test-piece with varying outer radius ρ_2, constant conductivity, and constant inner diameter, for various ratios of wall thickness to outside tube radius $(\rho_2 - \rho_1)/\rho_2$, Fig. 7.5. Solid lines (——) represent the complex impedance of the probe as a function of frequency, f. Broken lines (- - -) represent the effect of changing $(\rho_2 - \rho_1)/\rho_2$. The outermost solid curve applies for $\eta = 1$ and the innermost curve for $\eta = 0.9$, (7.14). Similar curves are obtained for a bobbin coil internal to a tube, Fig. 7.4 and (7.15) [8]

means that geometrical variations in a test-piece will be less noticeable to a probe operating at higher frequency, if all other parameters are equal.

Eddy-current inspection commonly needs to be done in regions where the geometrical variation of the test-piece is noticeable, however. Examples of such variations include edge effects. As a surface probe approaches the edge of a plate, as a bobbin probe emerges from a tube, or as a rotary probe emerges from a borehole, for example, there is a sharp transition in the eddy current density in the vicinity of the coil due to the truncation of the test-piece. The impedance changes in the eddy-current probe that result from changes in local test-piece geometry are often larger than impedance changes due to defects in those regions. The inspector therefore faces the problem of needing to separate a defect signal from a potentially masking signal due to geometrical variations of the test-piece.

This section offers a review of quasi-analytical solutions to problems that have been solved in relation to EC NDE of conductors with relatively sharp geometrical variations. Many of the solutions employ the truncated region eigenfunction expansion (TREE) method, introduced by Theodoulidis [9] and mentioned in Sect. 6.3.5 with reference to modeling the effect of a ferrite probe core on the probe impedance.

7.3.1 Truncated Region Eigenfunction Expansion Method

The TREE method is a quasi-analytical method of solving the electromagnetic equations governing probe coil behavior in the environs of conductive test-pieces of various geometries. The homogeneous and layered flat and cylindrical test-pieces treated in Chap. 6 and Sect. 7.2 were tractable by the traditional method of separation of variables, as employed by Dodd, Deeds, and Cheng [4–6]. The TREE method also relies upon separation of variables to express a general solution for the electromagnetic field in analytic form but, additionally, employs truncation of the solution domain in one or more coordinates. Truncation of the solution domain allows expression of the solution in the truncated coordinate as a series summation rather than as an integral of infinite extent. The primary advantage of this approach is that the interface conditions on the electromagnetic fields can be satisfied at several interfaces simultaneously, allowing analytical treatment of the eddy-current inspection of truncated conductors such as the ends of tubes or rods, and the edges of plates. The development of the TREE method and its application to several problems in EC NDE that were previously intractable analytically was a significant breakthrough in the field, carrying the additional benefit of highly efficient numerical solvers with easier error control than afforded by the numerical evaluation of integrals [10].

7.3.2 Wedge and Plate Edge

In a series of articles published in 2005 [11], 2010 [12], and 2014 [13], the problem of EC inspection of a thick conductor with an abrupt edge has been examined in different aspects. This test-piece geometry is also termed a *wedge* conductor or, in the case of a wedge with a right-angled vertex, a *quarter-space* conductor. The first of these articles was concerned with calculating the impedance of an eddy-current surface coil, whose axis is perpendicular to one of the faces of a conductive quarter space [11], Fig. 7.8. The second solved a similar problem but for a surface coil whose axis may adopt any of the three orthogonal directions relative to the faces of the quarter-space [12]. In a new departure, the focus of [13] was computation of the impedance of an EC coil in the vicinity of a conductive wedge of arbitrary angle. The assumptions adopted were that the wedge is perfectly conducting and that the coil axis is parallel to the line defining the vertex of the wedge. For this arrangement, the problem reduces to that of a tangent coil (Sect. 6.4) above a half-space conductor as the wedge angle tends to 180°.

In 2006, the TREE method calculation of eddy-current coil impedance for a coil with axis perpendicular to the surface of a truncated plate was published [14], Fig. 7.9. This result is particularly useful for understanding the contribution made by the edge of a plate to the EC coil impedance. Figure 7.10 shows a normalized impedance plane plot calculated as the coil is moved from the surface of a plate, over its edge, and to a point remote from it. The normalized impedance is plotted as a difference

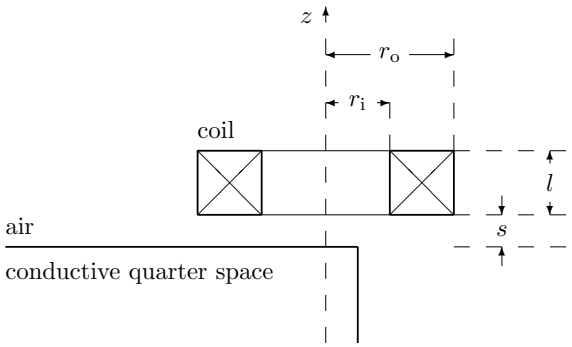

Fig. 7.8 Cross-section through the axis of a circular, air-cored, eddy-current coil, positioned horizontally above a conductive quarter-space

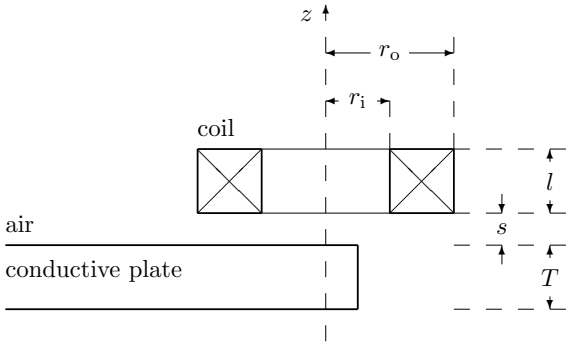

Fig. 7.9 Cross-section through the axis of a circular, air-cored, eddy-current coil, positioned horizontally above a conductive plate

relative to the free-space (isolated coil) value, with the maximum difference revealed when the coil is over the plate, at the lower end of each curve in the figure. Five plate thicknesses are considered in Fig. 7.10 and parameters of the calculation are given in Table 7.1.

Together, these solutions for EC coil interaction with wedge and plate-edge geometries represent a significant advance in the analysis of EC coil impedance due to sharp geometrical features for the reasons mentioned in Sec. 7.3.1.

7.3.3 End Effects and Cylindrical Conductors

The earliest application of the TREE method in the context of EC NDE was to the analysis of impedance of a surface coil with a ferrite core in the vicinity of a layered conductive half-space, Sect. 6.3.5, published in 2003 [9]. The core was treated as a truncated ferromagnetic cylinder. Building on this approach, a series of publications have treated a variety of test-pieces with truncated circular cylindrical geometry.

A quasi-analytical solution for the impedance of a bobbin coil emerging from the end of a tube, and coaxial with it, was published in 2004 [15]. The effects of wall-thinning near the tube end and the difficulty of detecting a small defect close

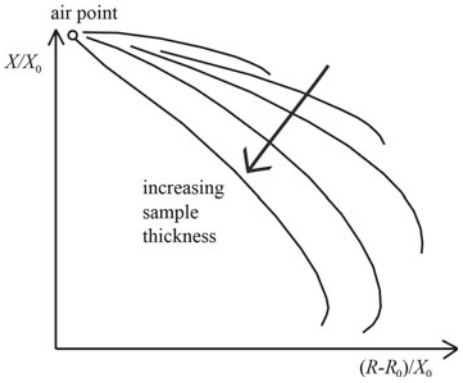

Fig. 7.10 Normalized impedance-plane plot for a coil with axis perpendicular to the surface of a plate, thickness T, as the coil scans from the plate to free space, over the plate edge (Fig. 7.9). Normalized impedance is plotted as a difference relative to the free-space (isolated coil) value, with the maximum difference revealed when the coil is over the plate, at the lower end of each curve [14]

Table 7.1 Parameters for the numerical calculations whose data are presented in Fig. 7.10 [14]

Coil parameters		Value
r_o	Outer radius (mm)	11.43
r_i	Inner radius (mm)	4.04
l	Length (mm)	8.02
s	Stand-off (mm)	1.08
n	Number of turns	1,858
Test-piece parameters		Value
σ	Conductivity (MSm^{-1})	17.5
μ_r	Relative permeability	1

to the tube end were demonstrated in this paper. The complementary problem, of an encircling coil coaxial with a truncated circular conducting rod, layered rod or tube, was treated in 2005 [16, 17].

A solution published in 2008 accommodated a greater degree of uncertainty in the position of the coil in relation to a borehole [18], modeling the impedance of both a rotary coil interior to the borehole, Fig. 6.5, and of a bobbin coil whose axis is offset from the axis of the borehole, Fig. 6.27.

The interested reader is invited to pursue these solutions through the original literature cited here.

7.4 Summary

This chapter has collected together analytical expressions for the impedance of a coil in the presence of layered, coated, or thin flat and cylindrical test-pieces. Impedance plane plots that show how the impedance varies as a function of various geometrical, physical, and probe parameters have been presented. Further, the Truncated Region Eigenfunction Expansion method has been mentioned as having been successfully applied to model the impedance of EC coils in the vicinity of test-pieces with sharp geometrical discontinuities.

Building upon the discussion of signals, coils, and the impedance responses to various types of test piece, covered in Chap. 6 and this chapter, the next chapter considers the ways in which coils and other sensors are put together in various configurations to form probes that are optimized for different inspection needs.

7.5 Examples

1. Identify *two* limiting cases in which the expression for the impedance of an EC surface coil positioned above a coated half-space conductor (7.5) should reduce to the result for the half-space conductor (given in (6.87) and reproduced below for convenience):

$$Z = \frac{j\omega\mu_0\pi n^2}{l^2(r_o - r_i)^2}\int_0^\infty \frac{J^2(\kappa r_i, \kappa r_o)}{\kappa^5}\left(2l + \frac{1}{\kappa}\left\{2e^{-\kappa l} - 2 + [e^{-2\kappa(l+s)} + e^{-2\kappa s} - 2e^{-\kappa(l+2s)}]\left(\frac{\gamma-\kappa}{\gamma+\kappa}\right)\right\}\right)d\kappa$$

   and show that (7.5) does indeed reduce correctly in those limits.
2. Identify one limiting case in which the expression for the impedance of an EC surface coil positioned above a plate conductor (7.6) should reduce to the result for the half-space conductor given above, and show that (7.6) does indeed reduce correctly in that limit.

References

1. Kolyshkin, A.A., Vaillancourt, R.: Impedance of a single-turn coil due to a double-layered sphere with varying properties. IEEE T. Magn. **31**, 2274–2280 (1995)
2. Theodoulidis, T.P., Kriezis, E.E.: Coil impedance due to a sphere of arbitrary radial conductivity and permeability profiles. IEEE T. Magn. **38**, 1452–1460 (2002)
3. Sabbagh, H.A., Murphy, R.K., Sabbagh, E.H., Aldrin, J.C., Knopp, J.S.: Computational Electromagnetics and Model-Based Inversion: A Modern Paradigm for Eddy-Current Nondestructive Evaluation. Springer, New York (2013)

4. Dodd, C.V., Deeds, W.E.: Analytical solutions to eddy-current probe-coil problems. J. Appl. Phys. **39**, 2829–2838 (1968)
5. Cheng, C.C., Dodd, C.V., Deeds, W.E.: General analysis of probe coils near stratified conductors Int. J. NDT **3**, 109–130 (1971)
6. Dodd, C.V., Cheng, C.C., Deeds, W.E.: Induction coils coaxial with an arbitrary number of cylindrical conductors. J. Appl. Phys. **45**, 638–647 (1974)
7. Cartz, L.: Nondestructive Testing: Radiography, Ultrasonics, Liquid Penetrant, Magnetic Particle. Eddy Current. ASM International, Materials Park, OH (1995)
8. McMaster, R.C., McIntire, P. (eds.), Mester, L.M. (tech. ed.): Nondestructive Testing Handbook: Electromagnetic Testing, vol. 4, 2nd edn. American Society for Nondestructive Testing, Columbus (1986)
9. Theodoulidis, T.P.: Model of ferrite-cored probes for eddy current nondestructive evaluation. J. Appl. Phys. **93**, 3071–3078 (2003)
10. Theodoulidis, T.P., Kriezis, E.E.: Eddy Current Canonical Problems (with Applications to Nondestructive Evaluation). Tech Science Press, Forsyth (2006)
11. Theodoulidis, T.P., Bowler, J.R.: Eddy current coil interaction with a right-angled conductive wedge. P. Roy. Soc. A-Math. Phy. **461**, 3123–3139 (2005)
12. Interaction of an eddy-current coil with a right-angled conductive wedge. IEEE T. Magn. **46**, 1034–1042 (2010)
13. Trampel, C.P., Bowler, J.R.: Eddy-current coil interaction with a perfectly conducting wedge of arbitrary angle. Res. Nondestruct. Eval. **25**, 186–202 (2014)
14. Bowler, J.R., Theodoulidis, T.P.: Coil impedance variation due to induced current at the edge of a conductive plate. J. Phys. D: Appl. Phys. **39**, 2862–2868 (2006)
15. Theodoulidis, T.: End effect modeling in eddy current tube testing with bobbin coils. Int. J. Appl. Electrom. **19**, 207–212 (2004)
16. Bowler, J.R., Theodoulidis, T.P.: Eddy currents induced in a conducting rod of finite length by a coaxial encircling coil. J. Phys. D: Appl. Phys. **38**, 2861–2868 (2005)
17. Sun, H.Y., Bowler, J.R., Theodoulidis, T.P.: Eddy currents induced in a finite length layered rod by a coaxial coil. IEEE T. Magn. **41**, 2455–2461 (2005)
18. Theodoulidis, T.P., Bowler, J.R.: Impedance of an induction coil at the opening of a borehole in a conductor. J. Appl. Phys. **103**, 024905 (2008)